Analyst

Microfluidic perfusion modulates growth and motor neuron differentiation of stem cell aggregates

Journal:	*Analyst*
Manuscript ID	AN-ART-03-2020-000491.R1
Article Type:	Paper
Date Submitted by the Author:	29-May-2020
Complete List of Authors:	Jackson-Holmes, Emily; Georgia Institute of Technology, Chemical & Biomolecular Engineering Schaefer, Amanda; Georgia Institute of Technology, Chemical & Biomolecular Engineering McDevitt, Todd; Gladstone Institutes, Gladstone Institute of Cardiovascular Disease Lu, Hang; Georgia Institute of Technology, Chemical and Biomolecular Engineering

ARTICLE

Microfluidic perfusion modulates growth and motor neuron differentiation of stem cell aggregates

-Received 00th January 20xx,
Accepted 00th January 20xx

DOI: 10.1039/x0xx00000x

Emily L. Jackson-Holmes,*[a] Amanda W. Schaefer, [a] Todd C. McDevitt, [b,c] and Hang Lu [a,d]

Microfluidic technologies provide many advantages for studying differentiation of three-dimensional (3D) stem cell aggregates, including the ability to control the culture microenvironment, isolate individual aggregates for longitudinal tracking, and perform imaging-based assays. However, applying microfluidics to studying mechanisms of stem cell differentiation requires an understanding of how microfluidic culture conditions impact cell phenotypes. Conventional cell culture techniques cannot directly be applied to the microscale, as microscale culture varies from macroscale culture in multiple aspects. Therefore, the objective of this work was to explore key parameters in microfluidic culture of 3D stem cell aggregates and to understand how these parameters influence stem cell behavior and differentiation. These studies were done in the context of differentiation of embryonic stem cells (ESCs) to motor neurons (MNs). We assessed how media exchange frequency modulates the biochemical microenvironment, including availability of exogenous factors (e.g., nutrients, small molecule additives) and cell-secreted molecules, and thereby impacts differentiation. The results of these studies provide guidance on how key characteristics of 3D cell cultures can be considered when designing microfluidic culture parameters. We demonstrate that discontinuous perfusion is effective at supporting stem cell aggregate growth. We find that there is a balance between the frequency of media exchange, which is needed to ensure that cells are not nutrient-limited, and the need to allow accumulation of cell-secreted factors to promote differentiation. Finally, we show how microfluidic device geometries can influence transport of biomolecules and potentially promote asymmetric spatial differentiation. These findings are instructive for future work in designing devices and experiments for culture of cell aggregates.

Introduction

Microfluidic tools provide enhanced capabilities for the study of stem cell aggregate differentiation[2-4]. For example, microfluidic techniques can be used to control different aspects of the culture microenvironment[5-7] or to perform imaging-based analyses on individual samples[8, 9]. However, exploring any of these applications requires an understanding of how microfluidic culture conditions impact cell behavior and differentiation. Conventional cell culture techniques and protocols cannot directly be applied to the microscale, as microscale culture varies from macroscale culture in ways that can critically affect cell behavior. One key difference in microscale culture is that the density of cells per volume of media is much higher, and this is particularly true for cell aggregates. This requires careful consideration of the method and frequency with which media exchange is performed, so that sufficient delivery of nutrients and removal of waste is achieved. Approaches to considering media exchange for two-dimensional (2D) cell culture in microfluidics have been proposed and discussed by Przybyla and Voldman[10], Young and Beebe[11], and Kim, et al.[12] These include choosing a media exchange interval or rate to match volumes typical of bulk culture conditions[10] or considering reaction and diffusion time scales of nutrient consumption and applying scaling arguments[11]. Regardless of the method used to estimate the required media exchange time scale, experimental validation is typically required, depending on the specific cell type and the microfluidic device configuration.

Previous work has explored different strategies for media exchange in microfluidic 2D stem cell cultures and has demonstrated how different strategies can have profound impacts on cell behavior. Media can be exchanged by perfusion either continuously or intermittently at defined intervals. The former strategy has been used as a way to regulate diffusible cell signaling and investigate its role in regulating cell behaviors[5, 13]. For example, autocrine and paracrine signaling are known to play important roles in stem cell self-renewal[14, 15], growth[16, 17], and differentiation[18]. Previous work using microfluidic perfusion based approaches has shown that cell-secreted signaling is critical for maintenance of mouse embryonic stem cell (mESC)

[a] School of Chemical & Biomolecular Engineering, Georgia Institute of Technology, Atlanta, GA, USA.
[b] Gladstone Institute of Cardiovascular Disease, Gladstone Institutes, San Francisco, CA, USA.
[c] Department of Bioengineering & Therapeutic Science, University of California San Francisco, San Francisco, CA, USA.
Parker H. Petit Institute for Bioengineering and Bioscience, Georgia Institute of Technology, Atlanta, GA, USA

pluripotency[13]. In contrast, periodic medium delivery, as opposed to continuous perfusion, has been shown to be an effective method for supporting cell growth and differentiation[19, 20]. Giobbe, et al. showed that in the context of human induced pluripotent (hiPSC) microfluidic culture, discontinuous media perfusion resulted in more homogenous colonies[6]. Furthermore, for differentiation towards each of the germ lineages, different discontinuous perfusion rates were found to be optimal. It has been shown that higher accumulation of cell-secreted factors promoted ectoderm and endoderm differentiation versus mesoderm, in contexts of spontaneous differentiation[6, 19]. Overall, studies such as these have provided insight into how microfluidic media exchange can be used to study and/or direct stem cell behavior.

While previous work has provided insight into how microfluidic media exchange conditions can be designed to have defined effects on 2D stem cell cultures, this has not been specifically explored for three-dimensional (3D) stem cell aggregate culture. It is well-known that there are distinct and important differences between 2D and 3D cell cultures[21]. In particular, there a few key differences that influence the design of microfluidic 3D stem cell culture systems. First, the geometry of a cell aggregate creates differences in how cells interact with one another and with soluble biochemical cues. A second key distinction is that, since 3D cultures have a higher density of cells per unit of culture area or volume, 3D cultures have different needs for the timescale and rate of nutrient delivery and waste removal. Finally, an important consideration is that microfluidic device geometries typically used to culture cell aggregates can affect media exchange. In the case of 2D microfluidic cell culture, cells are often grown in straight channels, where media can be exchanged by convective flow. In contrast, cell aggregates are often positioned within microfluidic traps or wells in order to isolate and track them throughout culture[1, 22, 23]. In these cases, media can either be exchanged convectively by flowing through the traps/wells, or it can be flowed through a main channel and exchanged by diffusion between the channel and the traps/wells.

Given these key considerations for designing 3D stem cell microfluidic culture systems, the objective of this work was to explore key parameters in microfluidic culture of stem cell aggregates and understand how these parameters influence stem cell behavior and differentiation. To accomplish this, we used a previously developed microfluidic device that provides the ability to culture, perturb, and observe individual stem cell aggregates[1]. The studies were performed by differentiating mESCs to progenitor motor neurons (pMNs). This differentiation protocol was chosen because it is well-established[24], motor neurons are a therapeutically relevant cell type, and in previous studies in plate cultures there is evidence for roles of cell-secreted signalling in promoting differentiation[25, 26]. Specifically, experimental studies were coupled with transport modelling to assess how media exchange frequency and device geometries modulate the biochemical microenvironment, including availability of exogenous factors (e.g., nutrients, small molecule additives) and cell-secreted molecules, and thereby impact differentiation. The results of these studies demonstrate that discontinuous perfusion is effective at supporting stem cell aggregate growth, in agreement with previous work with 2D cultures. We find that there is a balance between the frequency of media exchange, which is needed to ensure that cells are not nutrient-limited, and the need to allow accumulation of cell-secreted factors to promote differentiation. Finally, we find that microfluidic device geometries can be exploited as a tool to potentially expose aggregates to gradients of cell-secreted factors and promote spatial differentiation patterns.

Materials and Methods

Device Fabrication

Microfluidic devices were fabricated in polydimethylsiloxane (PDMS) (Dow Corning Sylgard 184, Midland, MI) by soft lithography.[27] Briefly, a master mold was fabricated by standard UV photolithography with the negative photoresist SU8-2100 (Microchem, Newton, MA) to create three layers of respective heights 200 µm, 100 µm, and 200 µm. Before PDMS molding, the master was treated with tridecafluoro-1,1,2,2-tetrahydrooctyl-1-trichlorosilane vapor (United Chemical Technologies, Bristol, PA) to allow release of the PDMS. To make devices, PDMS was mixed in a 10:1 ratio of pre-polymer and crosslinker, degassed to remove air bubbles, poured on the master mold, degassed a second time to remove remaining bubbles, and cured for 2 hours at 70 °C. Following curing, devices were cut and inlet and outlet holes for fluidic connections were punched with blunt needles (McMaster-Carr, Elmhurst, IL). Devices were then bonded onto glass coverslips by oxygen plasma bonding.

mESC Culture

G-Olig2 mESCs were obtained from ATCC® (ATCC SCRC-1037). These cells have green fluorescent protein (GFP) inserted into the gene for Olig2. Cells were maintained in tissue culture-treated polystyrene dishes (Corning Inc., Corning, NY) coated with 0.1% gelatin (Millipore, EmbryoMax). Undifferentiated culture media consisted of Dulbecco's modified Eagle's medium (DMEM) (Mediatech, Herndon, VA) supplemented with 15% fetal bovine serum (Hyclone, Logan, UT), 100 U/mL penicillin, 100 µg/mL streptomycin, 0.25 µg/mL amphotericin (Mediatech), 2 mM L-glutamine (Mediatech), 1x MEM non-essential amino acid solution (Mediatech), 0.1 mM 2-betamercaptoethanol (Fisher Scientific, Fairlawn, NJ), and 10^3 U/mL leukemia inhibitory factor (LIF) (ESGRO, Chemicon, Temecula, CA). Cells were passaged at approximately 70% confluence (typically every 2-3 days) and seeded at a density of 1 million cells for a 100 mm plate. Culture media was completely exchanged every other day.

Motor Neuron Differentiation of mESC Aggregates

A single cell suspension of undifferentiated mESCs was obtained by dissociating monolayer cultures with 0.05% trypsin-EDTA (Mediatech) for 3-4 minutes. Cells were resuspended in basal differentiation media that consisted of Dulbecco's modified Eagle's medium/nutrient mixture F-12 (DMEM/F12) (ThermoFisher Scientific) supplemented with 5% Knockout Serum Replacement (ThermoFisher Scientific), 1x Insulin-Transferrin-Selenium solution (ITS) (ThermoFisher Scientific), 1x MEM non-essential amino acid solution (Mediatech), 0.1 mM 2-betamercaptoethanol (Fisher Scientific, Fairlawn, NJ), 5 µM thymidine (Sigma-Aldrich), and 15 µM each of adenosine, cytosine, guanosine, and uridine (Sigma-Aldrich)[24].

Aggregates were formed by centrifugation (200 rcf) of mESCs into 400 µm agarose (OmniPur®, EMD Millipore) microwells placed within a 12-well tissue culture polystyrene plate (Corning, Inc.) as described previously.[28, 29] To yield 1000-cell aggregates, volumes of 0.5 mL of the single cell suspension (concentration: 2.4 million cells/mL) were added to each well of the 12-well plate. Cells were incubated in the wells in culture media for 18-24 hours to allow aggregates to form. Following formation, on day 1 aggregates were transferred either to microfluidic devices or petri dishes. Starting on day 2, media was supplemented with 1.5 or 4.5 µM Purpmorphamine (Pur) (Calciobiochem) and 2 or 6 µM Retinoic Acid (RA) (Sigma-Aldrich).

For batch suspension culture, aggregates were cultured in 100 mm bacteriological grade polystyrene Petri dishes (BD, Franklin Lakes, NJ) with approximately 2000 aggregates per plate in 10 mL of basal differentiation media. Plates were maintained on rotary orbital shakers (Benchmark Scientific, Edison, NJ) at a frequency of 45 rpm.[29, 30] Media was exchanged every other day, with 90% of the media replenished with fresh media. RA and Pur were supplemented starting at day 2 and with each additional media change.

Device Loading and Operation

Prior to each experiment all devices and tubing connections were sterilized by autoclaving. Components that could not be autoclaved were either purchased sterile or sterilized by ethylene oxide gas treatment. Devices were assembled with a 14 gauge dispensing tip with luer lock connection (McMaster-Carr) at the inlet. For priming devices with a syringe, a piece of silicone tubing (1/32" ID silicone tubing; Cole Parmer) was connected to the inlet using 18 gauge polypropylene dispensing needles (McMaster-Carr). For culture, a sterile 3 mL syringe (Becton Dickinson) with plunger removed was screwed onto the inlet to serve as media reservoir. At the device outlet, a blunt 16 gauge needle (McMaster-Carr) was connected to a length of silicone tubing. A pinch valve was placed on this tubing to allow pressurization of devices to remove bubbles. The silicone tubing was connected to a luer lock two-way stop cock (McMaster-Carr) using polypropylene needles, and then to an additional length of silicone tubing. Finally, a 0.2 µm syringe filter (VWR) was connected to the end of the outlet tubing with a polypropylene needle to provide a sterile barrier.

Prior to aggregate loading, devices were first primed with 70% ethanol using a syringe to remove air bubbles. Next, devices were rinsed with sterile phosphate-buffered saline (PBS) and then incubated with a 1 mg/ml bovine serum albumin (BSA; Millipore) solution for 30 minutes to passivate the surfaces.[31, 32] Finally, devices were rinsed with basal differentiation media. Aggregates were collected and resuspended at a concentration of approximately 600 aggregates/mL in a solution of 1.05 g/mL Percoll (Sigma Aldrich) in phosphate-buffered saline (PBS) to prevent rapid settling. Then, aggregates were pipetted into the inlet and loaded into devices via gravity-driven flow at approximately 1 ml/hr. Once aggregates were loaded, sterile gas permeable adhesive membranes were used to seal device inlets ("Breathe-Easier", Electron Microscopy Services). Device outlets were connected to a syringe pump (PHD 2000; Harvard Apparatus) and the entire setup was placed in a humidified incubator (HERAcell 240i, Thermo Scientific). During culture, devices were kept in a shallow, sterile water bath to limit evaporation. Devices were perfused at a defined flow rate and frequency by withdrawing differentiation media from a reservoir at the device inlet using the syringe pump. For continuous media perfusion conditions, media was withdrawn at a constant flow rate. For discontinuous media perfusion, media was completely exchanged within the device at defined time intervals; there was no media flow in devices except during media exchange.

Immunofluorescent Staining

Immunofluorescent staining was performed in devices by perfusing all solutions through the inlets by gravity-driven flow. For aggregates cultured in batch suspension, all steps were performed in 1.5 mL microcentrifuge tubes, and samples were continuously rotated on a tube rotator. First, samples were washed with PBS and fixed in 10% formalin at room temperature for 40 minutes. Following a wash in block buffer (2% BSA, 0.1% Tween 20, in PBS), samples were permeabilized in 1.5% Triton X 100 in PBS for 30 minutes. After washing in serum block buffer (2% goat serum, 0.1% Tween 20, in PBS) for 30 minutes, samples were incubated overnight at room temperature in the primary antibody solution: 1:20 Hb9 (81.5C10 from Developmental Studies Hybridoma Bank) in block buffer or 1:5 Nkx2.2 (74.5A5 from Developmental Studies Hybridoma Bank) in block buffer. The next day, samples were washed in serum block buffer for 30 minutes and then incubated in the secondary antibody solution (1:200 AlexaFluor 647 goat anti-mouse) at room temperature for 4 hours. Samples were washed a final time with serum block buffer for 30 minutes and imaged immediately. Device samples were imaged in devices; batch suspension culture samples were transferred to glass-bottom 24-well plates (MatTek Corporation) for imaging.

Confocal Microscopy

Samples were imaged on a confocal microscope (Zeiss LSM 700 Confocal Microscope) with a 20x objective. Z stacks were acquired to a depth of ~50 µm with spacings of 5 or 10 µm. For larger aggregates that did not fit in a single field of view, 2x2 tile scan images with 10% overlap were acquired and stitched together with the microscope software (ZEN, Zeiss). For live imaging in devices, device inlets were sealed with luer lock caps (McMaster-Carr) to maintain sterility.

Image Analysis

Confocal images from live and immunostained samples were analyzed using custom-written MATLAB code. For each aggregate, 5 slices with 10 µm spacing between optical sections were analyzed. Aggregates were first segmented manually from transmitted light images and the cross sectional area of each aggregate was measured. The aggregate diameter was calculated from the cross sectional area, assuming each cross section to be circular and using the formula for the diameter of a circle. The eccentricity was calculated using the "regionprops" function in MATLAB, defined as the ratio of the distance between the foci of the ellipse and the major axis length.

Individual cells were segmented based on Olig2 expression. The segmented aggregate image was first used to mask the image. To segment out individual cells, a modified version of a method developed by Lou et al. was used[33]. Starting from the greyscale image, contrast adjustment was performed as a preprocessing step. Next, a Gaussian filter was applied to the image, the Hessian matrix of the resulting image was calculated, and the first eigenvalue of the Hessian matrix was calculated. Then, a threshold was applied to the first eigenvalue of the Hessian matrix to eliminate dim pixel values that would otherwise result in poor segmentation. The resulting image was used as a mask to segment the contrast adjusted greyscale image. This typically yielded under-segmented cells, so a watershed transform was applied to the masked greyscale cells to yield a final, binary image of segmented cells.

To quantify Olig2 expression for each aggregate, the total pixel area of cells expressing that marker for all five z slices was calculated. To yield a metric for expression that was normalized by aggregate size, this value was then divided by the approximate volume of the portion of the aggregate that was imaged. The volume was calculated according to the formula $V = [(\pi\, h\text{^}2)/3] * (3r - h)$, where *h* was the height of the sampled region (50 µm) and *r* was the calculated radius of the aggregate. Finally, to compare across multiple conditions, marker expression was normalized by the mean expression level in batch cultures yield the final "Normalized Olig2 Expression".

To characterize asymmetry in Olig2 expression, the horizontal distance of each Olig2+ cell in an aggregate from the centerline of that aggregate was calculated and normalized to the aggregate radius. To take into consideration the position of each aggregate within its trap, a second metric was defined. For this metric, the horizontal distance of an Olig2+ cell from the trap entrance was calculated and was normalized by the total distance from the opening to back of the trap.

Statistical Analysis

Statistical analyses were performed using GraphPad Prism software. Statistical tests were performed using either a Mann-Whitney U test or non-parametric one-way ANOVA (with Kruskal-Wallis) combined with Dunn's multiple comparison's test for comparison of individual samples. P values less than 0.01 were considered significant.

Results and Discussion

Device Design Optimizations

To investigate the role of microfluidic culture parameters in differentiation of 3D mESC aggregates, a previously developed microfluidic device design[1] was adapted. This device provides the ability to observe individual stem cell aggregates over week-long cultures and to perturb the soluble culture microenvironment by changing the frequency of media delivery. In this work, the device design and external fluid handling components were modified to achieve two goals: (1) to improve aggregate loading and trapping, and (2) to facilitate confocal imaging at multiple time points (Figure 1 a,b; Supplemental Figure 1).

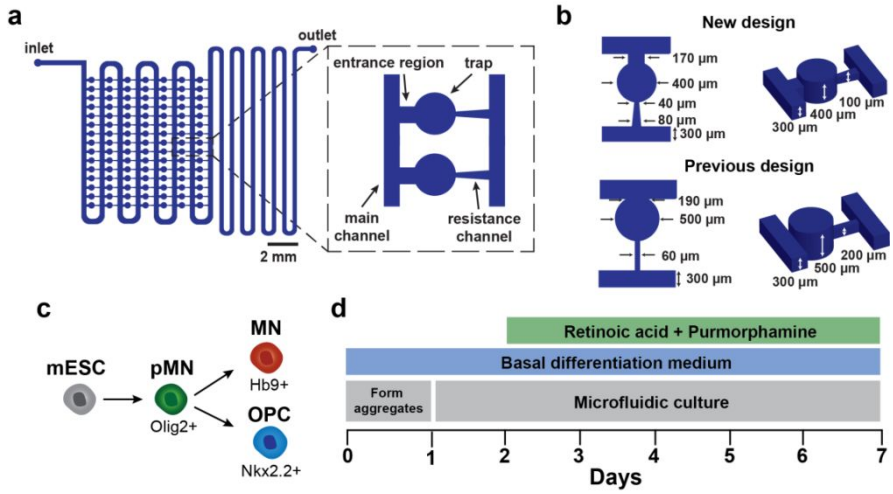

Figure 1. Experimental system overview. a) Design schematic of the microfluidic device, with inset depicting the main channel, trap, and resistance channel. b) Top and side view of trap geometries and dimensions, comparing the new, optimized trap geometries to those of the previously published design[1]. c) Cartoon depicts the differentiation of mESCs first to pMNs marked by Olig2 and then to either MNs or OPCs. d) Schematic of the differentiation protocol used.

To achieve the first goal, the geometry of the device was altered both to improve initial aggregate trapping and to improve maintenance of aggregate trapping during a long-term culture experiment. The original device design typically loaded with 50% of traps containing single aggregates, with remaining traps being empty or containing multiple aggregates[1]. It was observed experimentally that aggregates could deform and flow through the small resistance channel at the back of the trap, resulting in an empty trap. To address this challenge, the resistance channel initial width was reduced from 60 µm to 40 µm, and the height was reduced from 200 µm to 100 µm (Figure 1b). A consequence of decreasing the resistance channel dimensions was that it increased the overall trap fluidic resistance, and the ratio of fluidic resistance through the traps in relation to the main channel must be balanced for loading of traps[8, 9]. To offset the reduced resistance channel dimensions, the resistance channel shape was changed to be tapering from the initial width of 40 µm and the maximum width of 80 µm (with height remaining constant) (Figure 1b). This design provided the narrow 40 µm opening needed to minimize aggregates from entering but with a lower overall fluidic resistance than a 40 µm straight channel.

A second design change was implemented to decrease the occurrence of aggregates flowing out of the front of traps during culture if fluid flow disturbances occurred (for example, while attaching or detaching syringes to the device tubing). To address this, a narrowed rectangular region of width 170 µm and height 300 µm was added to the trap entrance (Figure 1b). The rationale was that as aggregates increased in size during culture, they would become physically constrained from exiting the trap upon exposure to minor flow disturbances. In another design change, the diameter and height of the trap were reduced from 500 µm to 400 µm (Figure 1b). Over the culture time period needed for these studies (one week), aggregates were not expected to grow larger than 400 µm. Reducing the trap size enabled a larger portion of the trap to be imaged within a single field of view and more traps to be packed in a smaller device footprint.

A final design change was made to improve control over the flow rate during aggregate loading. Devices are loaded using gravity-driven flow based on a height difference between inlet and outlet, and the previous device design needed to be coupled in series with a second identical device to increase the overall fluidic resistance to achieve the desired flow rate. To avoid the need to use a second device, a serpentine channel region was added to the end of the device to increase the overall fluidic resistance (Figure 1a). The optimal flow rate for loading was determined experimentally to be ~ 1 ml/hr. Together with all of the design changes, the loading efficiency was increased from 50% to 70% singly-loaded traps. In the new design, the ratio of trap to main channel resistance of the new design is ~ 6, compared to ~ 20 with the old design.

To achieve the second goal of facilitating confocal imaging during experiments, a number of external fluid handling components were added to the device to address experimental needs (Supplemental Figure 1). These components addressed requirements associated with device priming, device loading, maintaining sterility, and performing microscopy on live samples. Importantly, all fluid handling components could be sterilized by autoclaving, by ethylene oxide treatment, or were purchased sterile. These components are described in more detail in the Supplemental Information.

Differentiation under Continuous and Discontinuous Perfusion

To study the role of the media exchange method on 3D mESC motor neuron differentiation, mESC aggregates were differentiated according to an established protocol[24, 34]. Aggregates were formed from G-Olig2 mESCs in basal differentiation media and then cultured in devices or plate controls. Retinoic acid (RA) and the Sonic Hedgehog agonist, purmorphamine (Pur), were added to the media starting at day 2 and with every successive media change to promote motor neuron differentiation (Figure 1 c,d). The fluorescent reporter cell line enabled assessment of Olig2 expression, a

marker for progenitor motor neurons (pMNs), in live aggregates.

To extend previous studies of 2D microfluidic cell culture, we assessed whether discontinuous media perfusion would be more effective at supporting cell growth than continuous media perfusion in 3D microfluidic culture. We hypothesized that continuous perfusion may perturb necessary diffusible cell signalling. To test this, we compared discontinuous perfusion at a frequency of $f = 1\ d^{-1}$ (e.g. exchanging media once per day) to continuous perfusion at a rate of 10 µL hr^{-1} and assessed cultures at day 7 of differentiation. The day 7 time point was chosen based on preliminary experiments (not shown) indicating that this was when generation of Olig2+ pMNs could be observed.

To assess cell growth, we characterized aggregate size and morphology (Figure 2 a-c). The mean size of aggregates cultured at $f = 1\ d^{-1}$ was slightly smaller than plate controls, but this difference was not statistically significant. In contrast, aggregates cultured at 10 µL hr^{-1} were significantly smaller than plate controls ($p<0.0001$) (Figure 2b). As a descriptor of aggregate shape, eccentricity was calculated from bright field images Figure 2c). Aggregates cultured at $f = 1\ d^{-1}$ had less circular morphologies than plate controls ($p<0.01$). This is likely explained by our observation that aggregates were larger in this condition and could conform to segments of the trap wall, resulting in non-circular shapes. In contrast, aggregates cultured at 10 µL hr^{-1} were similar in shape to controls. As aggregates in this condition remained small, influences of trap shape seemed to have little to no effect. Overall, these data indicate that there were no statistically distinguishable differences in cell growth between cultures at $f = 1\ d^{-1}$ and plate controls, but growth under culture at 10 µL hr^{-1} was reduced. It is possible that the reduced cell growth was either a result of nutrient limitations or due to cell-secreted molecules necessary for cell growth being swept away by continuous perfusion. To explore which of these two possibilities explained the data, we assessed key transport parameters (Supplemental Information). We found that for both continuous and discontinuous media perfusion, the time scale of media exchange was faster than the time scale of cellular consumption of glucose, a key nutrient. This indicated that cells were likely not nutrient limited. Second, for continuous perfusion, we calculated the Peclet number (Pe) for transport of a cell-secreted molecule such as a growth factor. We found that Pe>>1 (Pe ≈ 850), indicating that convection dominates and thus that this continuous perfusion condition can indeed perturb cell-secreted paracrine signalling. We therefore hypothesized that reduced aggregate growth in culture under continuous perfusion was not due to nutrient restrictions, but rather due to perfusion-based removal of cell-secreted factors necessary for growth. This conclusion is corroborated by previous work with 2D cell culture that demonstrated inhibition of cell growth under continuous perfusion conditions[13]. These results highlight how nutrient delivery and allowing cell-secreted factors accumulate are inherently conflicting requirements that ultimately need to be

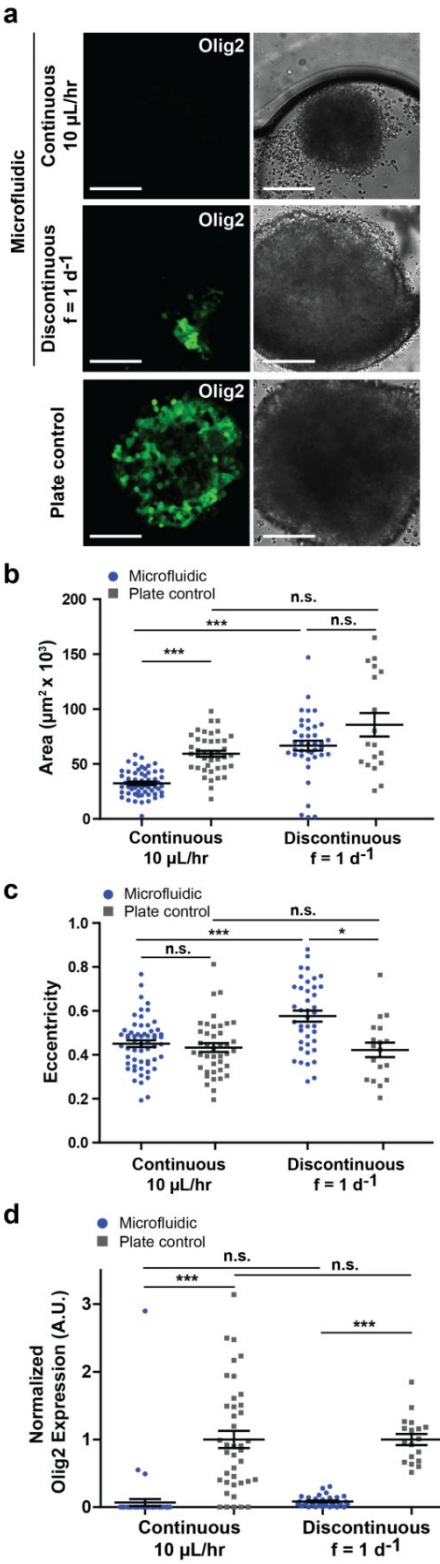

Figure 2. Effects of media perfusion method on morphology and pMN differentiation. a) Representative images from a single confocal slice of Olig2 expression at day 7 and corresponding transmitted light images. Scale bars = 100 µm. b) Aggregate cross-sectional area was measured from bright field images at day 7. c) Aggregate eccentricity was measured from bright field images at day 7. Continuous: n = 58 from 2 devices; Plate control: n = 41. Discontinuous: n = 67 from 2 devices; Plate control: n = 18. d) Normalized Olig2 expression quantified for each condition. Continuous: n = 58 from 2 devices; Plate control: n = 41 aggregates. Discontinuous: n = 37 from 1 device; Plate control: n = 18. Plate controls were n.s. Error bars represent SEM. Kruskal-Wallis test with Dunn's multiple comparisons was used. * indicates $p < 0.01$; *** indicates $p < 0.0001$.

balanced in designing operating conditions for a microfluidic device.

Next, to assess how the media exchange method impacted differentiation of mESCs to pMNs, we examined Olig2 expression at day 7 of culture under the same two conditions. As seen in the representative confocal microscopy images Figure 2a), little Olig2 expression was observed in both the $f = 1\ d^{-1}$ and 10 µL hr^{-1} conditions, whereas many Olig2+ cells were observed in plate controls. The amount of Olig2 expression for individual aggregates in each condition was quantified using image analysis (Figure 2d). Quantification revealed that there was no Olig2 expression in 10 µL hr^{-1} cultures, with the exception of three outlier aggregates. Examination of the data provided no obvious explanation for the existence of these outliers. Olig2 expression was slightly higher in $f = 1\ d^{-1}$ cultures, but the difference compared to 10 µL hr^{-1} was not statistically significant, likely due to the three outlying aggregates. For both perfusion conditions, Olig2 expression was much lower than plate controls ($p < 0.0001$).

We investigated whether there were any correlations between Olig2 expression and other parameters for $f = 1\ d^{-1}$ cultures. We did not assess 10 µL hr^{-1} cultures since Olig2 expression levels were barely detectable. We measured the correlation between Olig2 expression and aggregate size (Supplemental Figure 2a) by calculating the Spearman rank correlation, R. The Spearman correlation coefficient ranges from -1 to +1; values of +1, 0, and -1 indicate total positive, no, and total negative correlations, respectively. Based on this metric, aggregate size and Olig2 expression were not correlated for device cultures (R=0.033; n.s.) but were positively correlated for plate controls (R=0.66; p<0.001). We also assessed if there was a relationship between Olig2 expression of a given aggregate and its location in the device (Supplemental Figure 2b). Although there was variability in Olig2 expression among aggregates, there was no clear correlation with position.

Overall, these data indicate that both of these media exchange conditions do not promote differentiation of large populations of pMNs. For the continuous media perfusion condition, our results agree with previous literature and support the mechanism that continuous perfusion alters autocrine/paracrine signalling required both for growth and differentiation. However, the minimal pMN differentiation observed for $f = 1\ d^{-1}$ discontinuous perfusion was an unexpected result, so we next explored how additional perturbations of endogenous and exogenous signalling could influence pMN differentiation.

Effects of increasing RA and Pur Delivery on pMN Differentiation

Following the initial assessment of pMN differentiation under continuous and discontinuous perfusion, we hypothesized that lower effective concentrations of RA and Pur in microfluidic devices may have contributed to the minimal differentiation that was observed, as it is known that PDMS absorbs small molecules and hydrophobic molecules in particular[35, 36]. The tendency of PDMS to absorb a given molecule (the partition coefficient) is related to the logarithm of the octanol-water partition coefficient (logP) of that molecule[37]. In studies conducted by Wang et al.[37] and Auner, et al,[38] molecules with low logP values (<2.5[37] or <1.85[38]) exhibited low absorption into PDMS (<25% after 4.5 hours[37]) and molecules with high logP (>2.5[37] or >1.85[38]) exhibited high absorption (>75% after 0.5 hours[37]). RA and Pur have logP values of 6.30 (source: Sigma-Aldrich) and 7.58 (source: EPA[39]), respectively, and therefore are potentially highly absorbed by PDMS.

To evaluate whether increased delivery of RA and Pur to microfluidic cultures could promote increased pMN differentiation, we differentiated mESC aggregates under discontinuous perfusion at $f = 3\ d^{-1}$ (e.g. exchange media every 8 hours) at three-fold increased RA and Pur concentrations (6 µM and 4.5 µM, respectively). This condition was chosen to increase the total amount of RA and Pur delivered through both increased delivery frequency and concentration. The three-fold concentration increase was chosen to compensate for PDMS absorption of the molecules while also balancing the fact that there are upper limits to concentrations of these molecules at which adverse effects such as cell death occur. For comparison, we differentiated plate controls at both the original (2 µM RA; 1.5 µM Pur) and new concentrations (6 µM RA; 4.5 µM Pur).

To assess aggregate growth and morphology, we quantified aggregate cross-sectional area and eccentricity (Figure 3a-c). Aggregate size in $f = 3\ d^{-1}$ cultures was comparable to plate controls cultured at the same concentration but lower than plate controls cultured at the original RA and Pur concentrations (Figure 3b). We observe that increasing concentrations of RA and Pur affected cell growth. Quantification of eccentricity showed that aggregates cultured in devices displayed a less round morphology than both sets of plate controls (Figure 3c). This observation matched what was previously observed for $f = 1\ d^{-1}$ cultures—that aggregates tend to adopt the shape of portions of the trap as they grow, resulting in increased frequency of non-circular aggregate morphologies.

We next assessed the effects of increasing the total amount of RA and Pur delivery on differentiation of pMNs at day 7 (Figure 3a,d). We observed increased Olig2 expression in $f = 3\ d^{-1}$ cultures compared to $f = 1\ d^{-1}$ cultures, as shown in the representative images (Figure 3a). Quantification of Olig2 expression indicated that in $f = 3\ d^{-1}$ cultures the mean expression level was comparable to plate controls cultured at the same concentration of RA and Pur (6 µM RA; 4.5 µM Pur) but lower than the mean level of expression in plate controls cultured at the original RA and Pur concentrations (2 µM RA; 1.5 µM Pur) ($p<0.0001$; Figure 3b). Variability in the amount of Olig2 expression was observed across all experimental groups: aggregates cultured in devices at $f = 3\ d^{-1}$ displayed a range of expression levels, including a sub-population of aggregates with no Olig2 expression, and plate controls also exhibited a range of expression levels (Figure 3d).

As it is known that during differentiation pMNs generate both MNs and OPCs, we investigated whether these cell types

were generated in the $f = 3\ d^{-1}$ microfluidic cultures (Supplemental Information and Supplemental Figure 4). We found that pMNs gave rise to both committed MNs and OPCs in these cultures. In the microfluidic cultures, amounts of both cell types were lower than in plate controls, and in particular, microfluidic cultures showed very little differentiation of Nkx2.2+ OPCs.

We investigated whether there were any trends between Olig2 expression and other parameters for $f = 3\ d^{-1}$ cultures. Based on the Spearman rank correlation coefficient, aggregate size and Olig2 expression were significantly correlated for all three experimental groups: device cultures (R=0.34; p<0.001), plate controls at the same supplemented concentration (R=0.35; p<0.001), and plate controls at the lower concentration (R=0.44; p<0.01) (Supplemental Figure 3a). This suggested that Olig2 expression correlates with aggregate size, which is not surprising. We also assessed if there was a relationship between Olig2 expression of a given aggregate and its location in the device (Supplemental Figure 3b). Although there was variability in Olig2 expression among aggregates, as with $f = 1\ d^{-1}$ cultures, there was no clear correlation with position in the device.

The observation that pMN differentiation in microfluidic cultures increased when the total amount of RA and Pur delivery was increased supports the hypothesis that effective concentrations of these exogenous factors were likely lower in devices compared to plate controls. These small molecules are likely absorbed by PDMS[35, 36], and the data presented here suggests that this effect can be partially compensated for by increasing concentration and delivery frequency. In plate controls, we observed that the extent of pMN differentiation in plate controls was reduced by increasing concentrations of RA and Pur to 6 µM and 4.5 µM, respectively. This is not surprising, as previous work has shown that there are dose-dependent effects of Pur on numbers of Olig2+ pMNs generated[34]. Higher concentrations of Pur could result in adverse effects on cells or could promote differentiation of cells towards another non-pMN neural fate. Overall, our results suggest that PDMS absorption of RA and Pur can be partially compensated for by increasing concentration and frequency of delivery of the molecules.

Influence of Device Geometry and Transport on pMN Differentiation

For microfluidic-based culture and analysis of cell aggregates, device designs that incorporate physical traps or chambers[22, 23, 40-42] to isolate aggregates are frequently used because they prevent physical interactions between aggregates and enable observation of individual aggregates through time. However, in some cases the geometries of traps or chambers may influence the biochemical microenvironment, based on how they affect convective and diffusive transport of nutrients and exogenous and endogenous biomolecules. Therefore, we were interested in examining how geometrical features of our device could affect

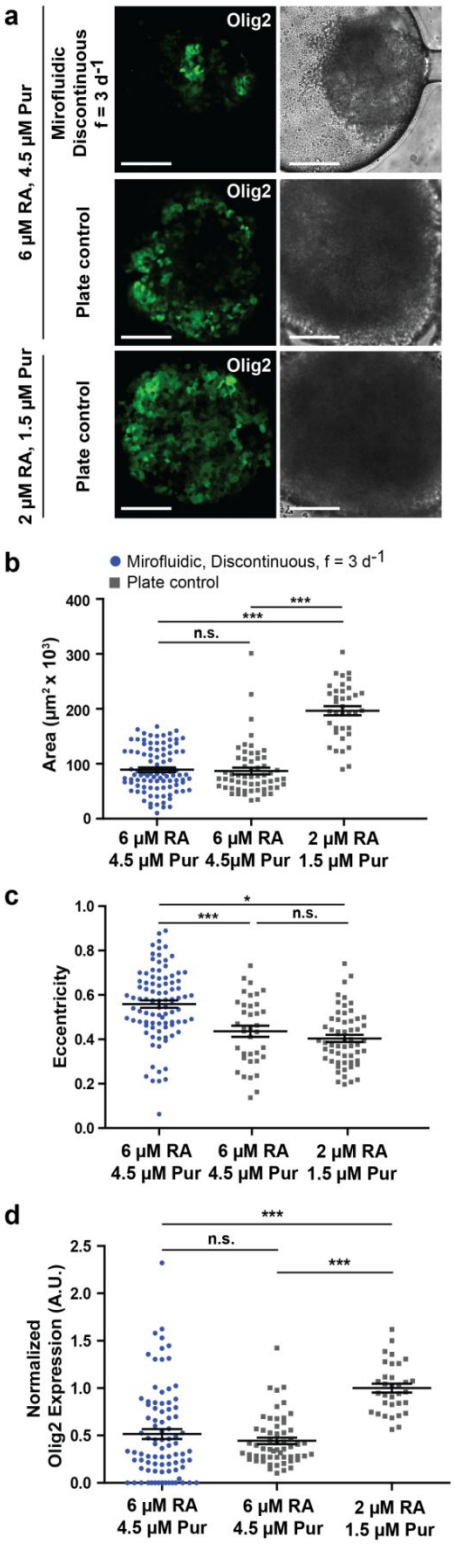

Figure 3. Effects of increased RA and Pur delivery on morphology and pMN differentiation. a) Representative images from a single confocal slice of Olig2 expression at day 7 and corresponding transmitted light images. Scale bars = 100 µm. b) Aggregate cross-sectional area was measured from bright field images at day 7. c) Aggregate eccentricity was measured from bright field images at day 7. b,c) Discontinuous device: n = 94 from 2 devices. Plate control (6 µM/4.5 µM): n = 58. Plate control (2 µM/1.5 µM): n = 37. d) Normalized Olig2 expression quantified for each condition. Discontinuous device: n = 91 from 2 devices. Plate control (6 µM/4.5 µM): n = 58. Plate control (2 µM/1.5 µM): n = 33. Error bars represent SEM. Kruskal-Wallis test with Dunn's multiple comparisons was used. * indicates < 0.01; *** indicates p < 0.0001

the soluble culture microenvironment and aggregate differentiation.

In our experimental data, we observed that Olig2+ cells were often localized in the region of aggregates closer to the back of the microfluidic trap. To quantify this observation, we examined data from two microfluidic culture conditions: discontinuous perfusion at $f = 1\ d^{-1}$ (with 2 μM RA, 1.5 μM Pur) and discontinuous perfusion at $f = 3\ d^{-1}$ (with 6 μM RA, 4.5 μM Pur). We quantified the horizontal distance of each Olig2+ cell in an aggregate from the centerline of that aggregate (Figure 4a). This value was normalized to the aggregate radius, calculated from the measured cross-sectional area. One caveat is that this analysis assumes that aggregates do not move or rotate in the traps over the course of culture, which we deemed to be reasonable based on experimental observations. In Figure 4b,d, the histograms show the relative frequency of Olig2+ cells at a given horizontal differentiation from the aggregate centerline, where 0 is the aggregate centerline, positive x values indicate cells closer to the trap entrance, and negative x values indicate cells closer to the back of the trap. The plots reflect population-level data from all aggregates for that condition. For aggregates cultured at $f = 1\ d^{-1}$, Olig2+ cells appeared to be localized in regions on both sides of the aggregate centerline, with a slightly larger peak of cells in regions closer to the backs of traps (Figure 4b). Assessment of histograms for individual aggregates (Supplemental Figures 6-9) showed that individual aggregate spatial distributions were varied.

We scored individual aggregates according to whether >50% of Olig2+ cells were in the front half of the aggregate (closer to the trap entrance), in the back half (closer to the trap back), or symmetrically distributed (i.e. an equal number of Olig2+ cells in each half of the aggregate). For aggregates cultured at $f = 1\ d^{-1}$, more aggregates (~55%) had >50% of Olig2+ cells localized in the back half (Figure 4c). For aggregates cultured at $f = 3\ d^{-1}$, an even larger proportion of

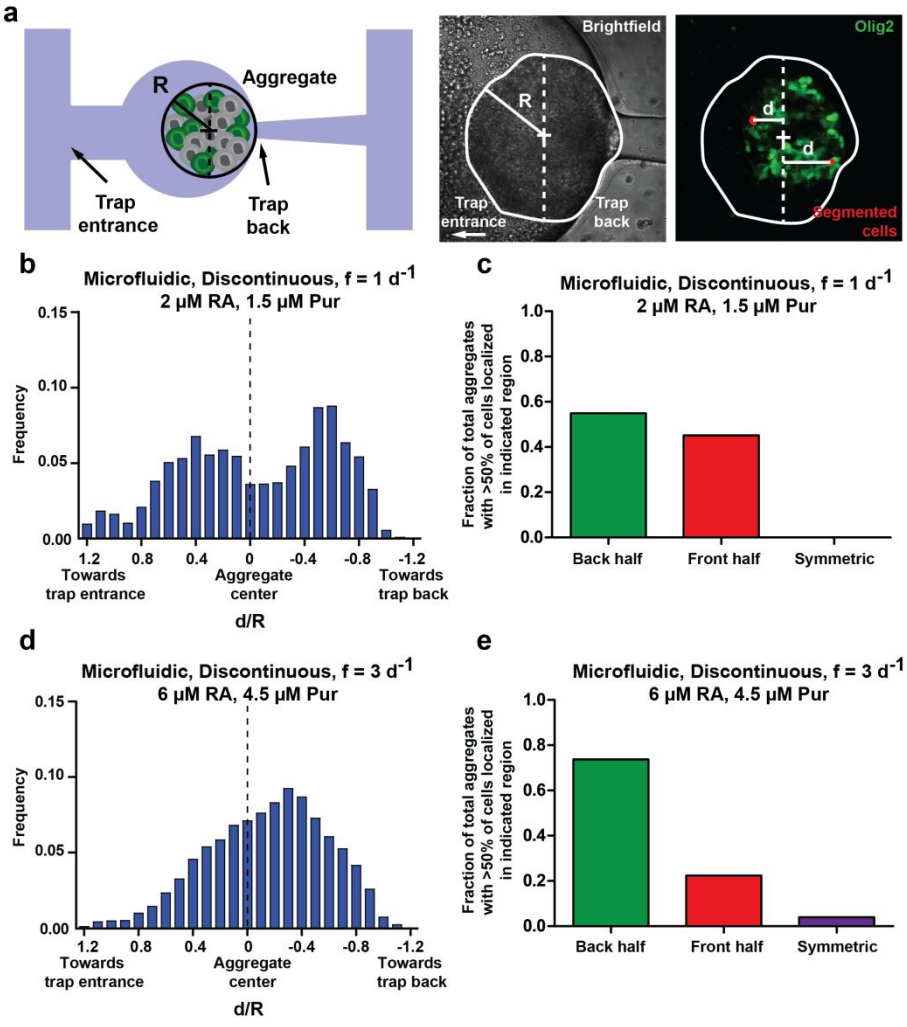

Figure 4. Effects of discontinuous perfusion frequency on spatial characteristics of Olig2 expression. a) Image describes how metric is quantified. Histograms show population-level data for horizontal position of Olig2+ cells with respect to aggregate center line for (b) discontinuous perfusion (f = 1 d^{-1}) with 2 μM RA and 1.5 μM Pur (n = 31 from 1 device) and (d) discontinuous perfusion (f = 3 d^{-1}) with 6 μM RA and 4.5 μM Pur (n = 47, representative of 2 devices). c,e) Graphs show the fraction of aggregates with >50% of Olig2+ cells in the front half of the aggregate (closer to the trap entrance), in the back half (closer to the trap back), or symmetrically distributed (i.e. an equal number of Olig2+ cells in each half of the aggregate).

Olig2+ cells were located in regions of aggregates closer to the backs of traps, potentially due to better overall differentiation of the aggregates under this flow condition (Figure 4d). This trend was also observed in individual aggregate distributions (Supplemental Figures 6-9), despite there being some variability among individual aggregates, with ~74% of aggregates having >50% of Olig2+ cells localized in the back half (Figure 4e). In contrast to microfluidic cultures, in plate controls at both RA and Pur concentrations Olig2+ cells were distributed roughly symmetrically throughout aggregates (Supplemental Figure 5). Note that the slight asymmetry in the distributions appeared to be a result of individual aggregate heterogeneity (Supplemental Figures 8-9). For all three experimental groups, manual curation of these data revealed no correlations between spatial location of Olig2 expression and parameters including aggregate size, aggregate position within trap, or aggregate position within the device.

Based on these experimental observations, we hypothesized that the asymmetric spatial distributions of Olig2 expression may be caused by spatial gradients of exogenous or endogenous factors in the traps. To assess if this was indeed a possibility, we used COMSOL to model mass transport and reaction in the system. We modelled the geometry of a single trap containing an aggregate (Supplemental Figures 10a and 11a) with cellular consumption/production of a representative nutrient, exogenously delivered small molecule and a secreted growth factor; we formulated the models under a no flow condition in order to assess the spatial distributions of concentrations between media exchanges (Supplemental Information and Supplemental Figures 10, 11). For the representative nutrient - glucose - the modelling results indicated that concentrations around the aggregate remained within ~98% of the inlet concentration during the time between media changes (up to 24 hours), which suggests that cells were exposed to sufficient nutrient levels (Supplemental Figure 10b-d). For a representative exogenously delivered small molecule, concentrations around the aggregate stayed within ~83% of the inlet concentration between media changes (Supplemental Figure 10e-h). Interestingly, for a representative cell-secreted growth factor, the modelling results indicated that asymmetric spatial distributions of the growth factor around the aggregate formed between media changes, with the peak concentration located in regions of the aggregate closer to the back of the trap (Supplemental Figure 11b-g. This was observed for a range of parameters including two different values for the growth factor consumption rate and three different values of the diffusion coefficient within the aggregate. This modelling supports the hypothesis that the asymmetric spatial distributions of Olig2 expression that were experimentally observed could be potentially caused by spatial gradients of endogenous cell-secreted factors in the traps.

Conclusions

This work explored how key microfluidic culture parameters influence stem cell aggregate growth and differentiation. 3D microfluidic cell cultures have distinct differences and culture requirements compared to 2D cultures due to the 3D nature, the cell density, and the surface area to volume ratio. This work provides an instructive example of how these key differences can be considered when designing microfluidic culture parameters. Specifically, we found that the media exchange strategy was a key determinant in modulating cell growth and differentiation of mESCs to pMNs. Continuous media perfusion resulted in less cell growth and minimal generation of pMNs, which is likely due to modulation of diffusible autocrine/paracrine signalling and not a consequence of nutrient limitations. This finding is in agreement with previous independent studies with 2D cultures[5, 6, 13]. Differentiation under discontinuous media perfusion was shown to promote differentiation of pMNs, although not to the level of plate controls. In addition, the discontinuous media perfusion frequency and concentrations of small molecules added to the media were identified as critical parameters influencing the extent of pMN differentiation. These findings provide a basis for understanding how microfluidic media exchange conditions modulate growth and differentiation of 3D mESC aggregates.

These studies also highlighted a disadvantage of using PDMS as a material for microfluidic cell culture. It is well-known that PDMS can absorb small molecules, particularly hydrophobic molecules[36]. Alternative strategies include treating PDMS to reduce absorption. Incubation of PDMS with BSA[43] or Pluronic has been used but is not fully sufficient to reduce absorption of molecules[36]. As an alternative, Gomez-Sjoberg et al. demonstrated that sol-gel treatment reduces absorption of drugs into PDMS[44, 45]. Material alternatives to PDMS such as polystyrene and cyclic olefin polymers/co-polymers can also be used in microfluidic cell culture, and although fabrication in these materials is becoming significantly easier[46-49], it remains more difficult and expensive. There are many trade-offs to be considered when selecting a material for microfluidic cell culture, and the many advantages of using PDMS, including optical clarity, ease of fabrication, and cost, still make it an attractive material for use in microfluidic devices for cell culture. Our results suggest that PDMS absorption of small hydrophobic molecules can be partially compensated for by increasing concentration and frequency of molecular delivery. This approach, combined with surface treatment of PDMS, could be used in the future to potentially mitigate PDMS absorption of hydrophobic molecules in cell culture studies.

Finally, these studies explored how asymmetrical microfluidic device geometries can potentially influence cell phenotypes spatially. Our experimental and transport modelling results suggest that gradients of endogenously secreted factors can potentially form in devices with asymmetrically geometries, such as ours, and that these may affect cell behaviour. This finding is instructive for future work in designing devices and experiments for culture of cell aggregates. Strategies to mitigate this challenge include recirculating media in devices and modifying the trap geometry. In addition, this phenomenon can potentially be

exploited to spatially pattern stem cell aggregates during differentiation. This latter feature has implications for studying spatial patterning of tissues and understanding how symmetry-breaking events occur during embryonic development.

Conflicts of interest

There are no conflicts to declare.

Acknowledgements

We acknowledge Dr. Raymond Swetenburg and Dr. Jessica Butts for help with the motor neuron differentiation protocol. We thank Dr. Chad Glen for helpful discussions on the data analysis methods. We thank Drs. Melissa Kemp, Victor Breedveld, and Mark Styczynski for useful discussions. Funding for this work was provided by the NSF Emergent Behaviors of Integrated Cellular Systems Science and Technology Center (CBET 0939511) and the Marcus Center for Therapeutic Cell Characterization and Manufacturing and Georgia Tech. HL is partially supported by NSF (1764406, 1707401) and NIH (AG056436, DC015652, NS096581, GM088333, EB021676). EJH was previously supported by an NSF Graduate Research Fellowship (DGE-1650044). AWS was supported by the Petit Undergraduate Research Scholars Program.

Notes and references

1. E. L. Jackson-Holmes, T. C. McDevitt and H. Lu, *Lab Chip*, 2017, **17**, 3634-3642.
2. S. E. Park, A. Georgescu and D. Huh, *Science*, 2019, **364**, 960-965.
3. B. Zhang, A. Korolj, B. F. L. Lai and M. Radisic, *Nature Reviews Materials*, 2018, **3**, 257-278.
4. Š. Selimović, H. Kaji, H. Bae and A. Khademhosseini, in *Microfluidic Cell Culture Systems (Second Edition)*, eds. J. T. Borenstein, V. Tandon, S. L. Tao and J. L. Charest, Elsevier, 2019, DOI: https://doi.org/10.1016/B978-0-12-813671-3.00002-5, pp. 31-63.
5. K. Blagovic, L. Y. Kim and J. Voldman, *PLOS ONE*, 2011, **6**, e22892.
6. G. G. Giobbe, F. Michielin, C. Luni, S. Giulitti, S. Martewicz, S. Dupont, A. Floreani and N. Elvassore, *Nat Methods*, 2015, **12**, 637-640.
7. J. Zhang, X. Wei, R. Zeng, F. Xu and X. Li, *Future Science OA*, 2017, **3**, FSO187.
8. K. Chung, Y. Kim, J. S. Kanodia, E. Gong, S. Y. Shvartsman and H. Lu, *Nat Methods*, 2011, **8**, 171-176.
9. K. Chung, C. A. Rivet, M. L. Kemp and H. Lu, *Analytical chemistry*, 2011, **83**, 7044-7052.
10. L. Przybyla and J. Voldman, *Annu Rev Anal Chem (Palo Alto Calif)*, 2012, **5**, 293-315.
11. E. W. Young and D. J. Beebe, *Chem Soc Rev*, 2010, **39**, 1036-1048.
12. L. Kim, Y. C. Toh, J. Voldman and H. Yu, *Lab Chip*, 2007, **7**, 681-694.
13. L. M. Przybyla and J. Voldman, *Proceedings of the National Academy of Sciences of the United States of America*, 2012, **109**, 835-840.
14. D. ten Berge, D. Kurek, T. Blauwkamp, W. Koole, A. Maas, E. Eroglu, R. K. Siu and R. Nusse, *Nat Cell Biol*, 2011, **13**, 1070-1075.
15. S. C. Bendall, M. H. Stewart, P. Menendez, D. George, K. Vijayaragavan, T. Werbowetski-Ogilvie, V. Ramos-Mejia, A. Rouleau, J. Yang, M. Bosse, G. Lajoie and M. Bhatia, *Nature*, 2007, **448**, 1015-1021.
16. K. Ogawa, A. Saito, H. Matsui, H. Suzuki, S. Ohtsuka, D. Shimosato, Y. Morishita, T. Watabe, H. Niwa and K. Miyazono, *Journal of Cell Science*, 2007, **120**, 55-65.
17. N. Mittal and J. Voldman, *Stem Cell Res*, 2011, **6**, 168-176.
18. B. G. Chung, L. A. Flanagan, S. W. Rhee, P. H. Schwartz, A. P. Lee, E. S. Monuki and N. L. Jeon, *Lab Chip*, 2005, **5**, 401-406.
19. G. G. Giobbe, M. Zagallo, M. Riello, E. Serena, G. Masi, L. Barzon, B. Di Camillo and N. Elvassore, *Biotechnol Bioeng*, 2012, **109**, 3119-3132.
20. E. Cimetta, E. Figallo, C. Cannizzaro, N. Elvassore and G. Vunjak-Novakovic, *Methods*, 2009, **47**, 81-89.
21. X. Li, A. V. Valadez, P. Zuo and Z. Nie, *Bioanalysis*, 2012, **4**, 1509-1525.
22. C. Y. Fu, S. Y. Tseng, S. M. Yang, L. Hsu, C. H. Liu and H. Y. Chang, *Biofabrication*, 2014, **6**, 015009.
23. M. Khoury, A. Bransky, N. Korin, L. C. Konak, G. Enikolopov, I. Tzchori and S. Levenberg, *Biomed Microdevices*, 2010, **12**, 1001-1008.
24. H. Wichterle, I. Lieberam, J. A. Porter and T. M. Jessell, *Cell*, 2002, **110**, 385-397.
25. R. Mizuguchi, M. Sugimori, H. Takebayashi, H. Kosako, M. Nagao, S. Yoshida, Y. Nabeshima, K. Shimamura and M. Nakafuku, *Neuron*, 2001, **31**, 757-771.
26. B. G. Novitch, A. I. Chen and T. M. Jessell, *Neuron*, 2001, **31**, 773-789.
27. G. M. Whitesides, E. Ostuni, S. Takayama, X. Jiang and D. E. Ingber, *Annual Review of Biomedical Engineering*, 2001, **3**, 335-373.
28. M. D. Ungrin, C. Joshi, A. Nica, C. Bauwens and P. W. Zandstra, *PLoS ONE*, 2008, **3**, e1565.
29. M. A. Kinney, R. Saeed and T. C. McDevitt, *Integr Biol (Camb)*, 2012, **4**, 641-650.
30. R. L. Carpenedo, C. Y. Sargent and T. C. McDevitt, *Stem cells*, 2007, **25**, 2224-2234.
31. C. Kim, K. S. Lee, J. H. Bang, Y. E. Kim, M. C. Kim, K. W. Oh, S. H. Lee and J. Y. Kang, *Lab Chip*, 2011, **11**, 874-882.
32. Y. H. Chen, C. C. Peng and Y. C. Tung, *Biomicrofluidics*, 2015, **9**, 054111.
33. X. Lou, M. Kang, P. Xenopoulos, S. Munoz-Descalzo and A. K. Hadjantonakis, *Stem Cell Reports*, 2014, **2**, 382-397.
34. D. A. McCreedy, C. R. Rieger, D. I. Gottlieb and S. E. Sakiyama-Elbert, *Stem Cell Res*, 2012, **8**, 368-378.
35. K. J. Regehr, M. Domenech, J. T. Koepsel, K. C. Carver, S. J. Ellison-Zelski, W. L. Murphy, L. A. Schuler, E. T. Alarid and D. J. Beebe, *Lab Chip*, 2009, **9**, 2132-2139.
36. M. W. Toepke and D. J. Beebe, *Lab Chip*, 2006, **6**, 1484-1486.
37. J. D. Wang, N. J. Douville, S. Takayama and M. ElSayed, *Annals of biomedical engineering*, 2012, **40**, 1862-1873.

38. A. W. Auner, K. M. Tasneem, D. A. Markov, L. J. McCawley and M. S. Hutson, *Lab on a Chip*, 2019, **19**, 864-874.
39. United States Environmental Protection Agency, Chemistry Dashboard: Purmorphamine, https://comptox.epa.gov/dashboard/dsstoxdb/results?search=DTXSID20415293, (accessed 05/01/2018).
40. J. Ruppen, L. Cortes-Dericks, E. Marconi, G. Karoubi, R. A. Schmid, R. Peng, T. M. Marti and O. T. Guenat, *Lab Chip*, 2014, **14**, 1198-1205.
41. S. Suri, A. Singh, A. H. Nguyen, A. M. Bratt-Leal, T. C. McDevitt and H. Lu, *Lab Chip*, 2013, **13**, 4617-4624.
42. M. Astolfi, B. Peant, M. A. Lateef, N. Rousset, J. Kendall-Dupont, E. Carmona, F. Monet, F. Saad, D. Provencher, A. M. Mes-Masson and T. Gervais, *Lab Chip*, 2016, **16**, 312-325.
43. E. Ostuni, R. G. Chapman, R. E. Holmlin, S. Takayama and G. M. Whitesides, *Langmuir : the ACS journal of surfaces and colloids*, 2001, **17**, 5605-5620.
44. R. Gomez-Sjoberg, A. A. Leyrat, B. T. Houseman, K. Shokat and S. R. Quake, *Analytical chemistry*, 2010, **82**, 8954-8960.
45. G. T. Roman and C. T. Culbertson, *Langmuir : the ACS journal of surfaces and colloids*, 2006, **22**, 4445-4451.
46. D. J. Guckenberger, T. E. de Groot, A. M. Wan, D. J. Beebe and E. W. Young, *Lab Chip*, 2015, **15**, 2364-2378.
47. A. M. D. Wan, A. Sadri and E. W. K. Young, *Lab on a Chip*, 2015, **15**, 3785-3792.
48. D. Konstantinou, A. Shirazi, A. Sadri and E. W. K. Young, *Sensors and Actuators B: Chemical*, 2016, **234**, 209-221.
49. T. Nguyen, S. H. Jung, M. S. Lee, T. E. Park, S. K. Ahn and J. H. Kang, *Lab Chip*, 2019, **19**, 3706-3713.

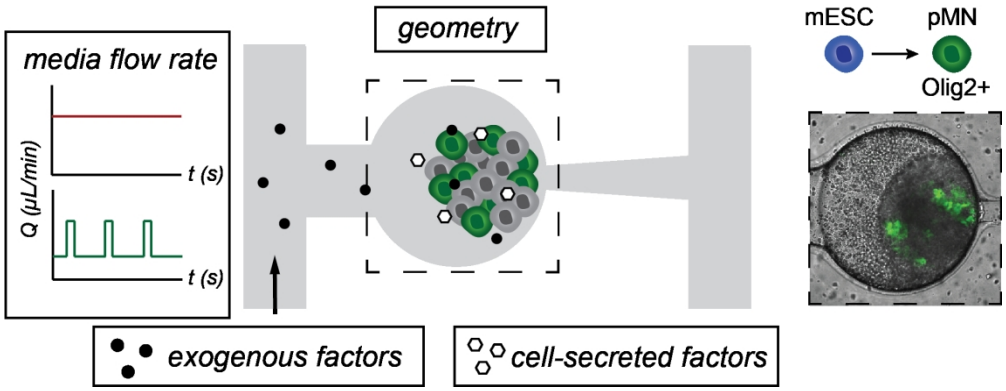
media flow rate
Q (μL/min)
t (s)
t (s)
geometry
mESC
pMN
Olig2+
exogenous factors
cell-secreted factors